DESIGN AND PERFORMANCE OF THE SYNCHRONIZATION SYSTEM AND BEAM DIAGNOSTIC INSTRUMENTS FOR SACLA

Hirokazu Maesaka#, Hiroyasu Ego, Chikara Kondo, Takashi Ohshima, Tatsuyuki Sakurai, Yuji Otake, RIKEN SPring-8 Center, 1-1-1 Kouto, Sayo-cho, Sayo-gun, Hyogo, Japan
Naoyasu Hosoda, Shin'ichi Matsubara, Ken'ichi Yanagida, JASRI/SPring-8, 1-1-1 Kouto, Sayo-cho, Sayo-gun, Hyogo, Japan
Shinobu Inoue, SPring-8 Service Co. Ltd., 1-20-5 Kouto, Shingu-cho, Tatsuno-shi, Hyogo, Japan

Abstract

In the x-ray free electron laser (XFEL) facility "SACLA", stable timing and rf signals with less than 100 fs stability are demanded. In addition, precise beam monitors with micron-meter-level spatial resolution and femtosecond-level temporal resolution are required. For the synchronization, we employed a low-noise master oscillator, an optical rf distribution system, IQ (In-phase and Quadrature) modulators/demodulators etc. For the beam diagnostics, we developed a sub-μm resolution rf cavity BPM, a few-μm resolution beam profile monitor, a C-band transverse rf deflecting structure for a 10 fs resolution temporal bunch structure measurement, etc. We confirmed the performance of these instruments by using an electron beam and finally achieved XFEL lasing in the wavelength region from 0.08 nm to 0.16 nm. Some possible applications of our instruments to an ERL are also discussed.

INTRODUCTION

The x-ray free-electron laser (XFEL) facility "SACLA" (SPring-8 Angstrom Compact Free Electron Laser) is a SASE (Self-Amplified Spontaneous Emission) FEL machine in the wavelength region around 0.1 nm. The construction of SACLA was completed in February, 2011 and the first x-ray lasing was achieved in June, 2011 [1].

The SACLA facility consists of an 8 GeV linear accelerator, in-vacuum undulators and an x-ray beamline, as shown in Fig. 1. An electron beam emitted from a thermionic gun is accelerated up to 8 GeV by 238 MHz, 476 MHz, L-band (1428 MHz), S-band (2856 MHz), and C-band (5712 MHz) accelerators. In the meantime, the temporal bunch length is compressed from 1 ns to 30 fs by three-stage bunch compressors (BC) in order to obtain the demanded peak current of 3 kA. The normalized emittance of the beam is approximately 1 mm mrad. The repetition rate of the accelerator is 60 Hz, synchronized to the AC power line frequency.

For a synchronization issue, the acceleration rf field should be stable within 1×10^{-4} for the amplitude and within 100 fs for the time-equivalent value of a phase. In addition, there are about 70 acceleration rf units and 20 other rf electronics, such as beam monitor circuits and user experiment stations, along the 700 m facility. Therefore, the rf and timing signals should be distributed over 700 m. We use an optical rf and timing distribution system for this demand, because an optical fiber has much smaller attenuation than a coaxial cable. To control the rf field for each accelerator unit precisely, we developed a low-level rf (LLRF) control system. The LLRF system consists of IQ (In-phase and Quadrature) modulators and demodulators, VME D/A and A/D converter boards etc.

For beam diagnostics, high-resolution beam monitors are necessary for both spatial and temporal measurements. The beam position is demanded to be monitored with sub-μm resolution, since an electron beam must be overlapped with x-rays within a few μm in the undulator section to generate SASE-FEL. The spatial resolution of a transverse beam profile image is also required with a few μm to see tiny electron beam of about a 10 μm rms radius. For the temporal profile measurements, the required resolution is 10 fs level, because the bunch length is compressed up to 30 fs.

In this paper, we describe the design and performance of each component in the synchronization and beam diagnostic system. Finally, we discuss possible applications for an ERL.

SYNCHRONIZATION SYSTEM

The synchronization system of SACLA [2] can be divided into an optical rf and timing distribution system and a LLRF system, as illustrated in Fig. 2. In the following subsections, the design and performance of these systems are described. In addition, we developed a special water-cooled enclosure and a low-noise DC power supply to reduce the temperature drift and power supply noise. The performances of these instruments are also described.

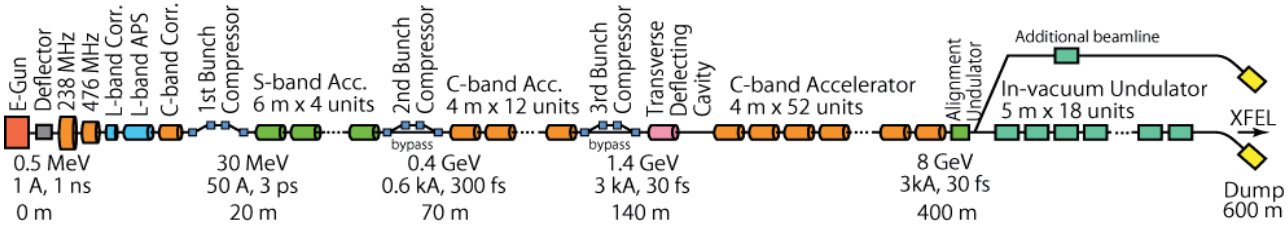

Figure 1: Schematic layout of the SACLA facility.

#maesaka@spring8.or.jp

ISBN 978-3-95450-145-8

Copyright © 2013 CC-BY-3.0 and by the respective authors

Optical RF and Timing Distribution System

A schematic block diagram of the optical rf and timing distribution system [2] is shown in Fig. 3. Low-noise rf signals of 5712 MHz and their sub-harmonics are generated by a low-noise master oscillator. Each signal is converted to a sinusoidally-modulated optical signal by an electrical-to-optical (E/O) converter consisting of a distributed feedback (DFB) laser diode and a $LiNbO_3$ Mach-Zehnder modulator. The wavelength of the carrier light is approximately 1550 nm. Trigger signals are also generated by a master trigger generator [3] and converted to a 5712 MHz phase shift keying (PSK) signal. The PSK signal is then converted to an optical signal.

These optical signals are combined into one optical fiber by wavelength-division multiplexing (WDM) technique. The combined signal is amplified by an erbium-doped fiber amplifier (EDFA) and distributed to accelerator components through phase-stabilized optical fibers (PSOF). The temperature coefficient of the PSOF is 2 ppm, which is much less than that of conventional optical fibers. At the receiver, the WDM optical signal is divided into individual wavelengths and converted to the electric rf and timing signals by fast photo-diodes in the optical-to-electrical (O/E) converter, respectively.

In addition, we are planning to install length-stabilized fiber links [4] in order to compensate for the path-length drift of the PSOFs. A frequency-stabilized laser is transmitted to a receiver as a length standard and reflected back to the transmitter with a Faraday rotator mirror. The fiber length is measured with a Michelson interferometer with sub-micron resolution. The length information is fed back to a variable delay line, such as a piezo-electric fiber stretcher. In this link, a 5712 MHz rf signal is also transmitted as a time reference. The phase drift of the signal transmitted in the PSOF is monitored at the receiver side by using an rf phase detector for 5712 MHz signals, and the PSOF length is controlled with the fiber stretcher. The length-stabilized link will be installed in 2012.

We measured the single-sideband (SSB) phase noise before and after the optical transmission in order to confirm whether the time jitter was sufficient or not. The result is plotted in Fig. 4. The time jitter after the transmission was calculated to be approximately 10 fs (rms) from the integration of the obtained phase noise spectrum.

We also tested the fiber length stabilization system by using a 1 km long fiber along the SPring-8 storage ring. The spectra of the fiber length stability for a free-run case and a stabilized case are plotted in Fig. 5. The fiber length fluctuation of less than 100 Hz was significantly reduced. The fiber length drift was stabilized to be less than 1 μm.

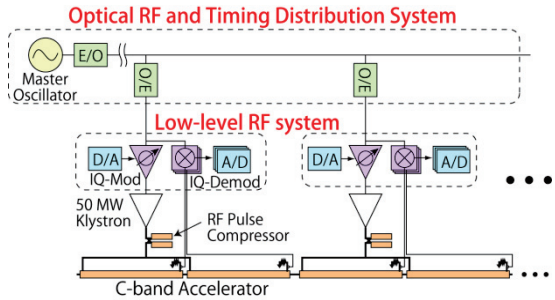

Figure 2: Schematic diagram of the synchronization system.

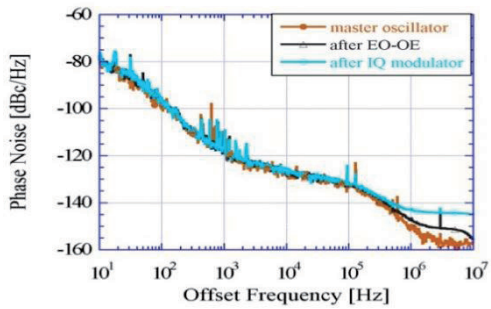

Figure 4: Phase noise spectra before and after the optical signal transmission. The carrier frequency is 5712 MHz. Brown, black and blue curves show the phase noise spectra of the master oscillator, after the E/O and O/E converters, and after the IQ modulator, respectively.

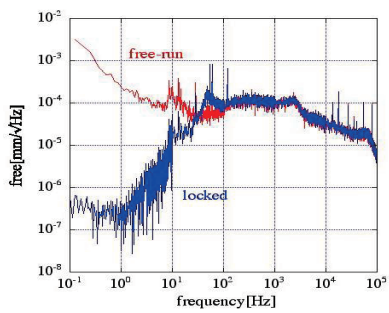

Figure 5: FFT spectra of the fiber length fluctuation from the fiber length stabilization experiment. The red line is the spectrum in the free-run case and the blue line is in the stabilized case.

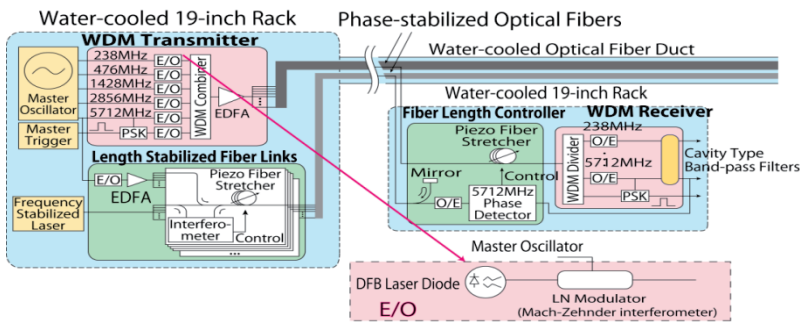

Figure 3: Block diagram of the optical rf and timing distribution system.

ISBN 978-3-95450-145-8

Copyright © 2013 CC-BY-3.0 and by the respective authors

Low-level RF Control System

A schematic diagram of the LLRF control system for each C-band accelerator unit is shown in Fig. 6. A time-reference rf signal is provided from an O/E converter and an acceleration rf signal with appropriate phase and amplitude is generated with an IQ modulator. IQ baseband waveforms are generated with a VME 238MHz 14-bit D/A converter board [5]. The rf signal is amplified with a solid-state amplifier and a 50 MW klystron, and fed into accelerating structures. A tiny part (10^{-6}) of the rf power around the accelerator cavity is picked up and detected with an IQ demodulator. The detected IQ baseband waveforms are recorded with a VME 238MHz 12-bit or 16-bit A/D converter board [5]. To reduce slow drifts of the acceleration rf phase, the detected signal is fed back to the D/A converter with PID (Proportional-Integral-Derivative) feedback control algorithm.

Figure 7 shows some waveforms of an acceleration rf field taken with the IQ demodulator for the C-band accelerator. For the stability issue, a trend graph of the phase of the 238 MHz sub-harmonic buncher cavity, which was taken with the IQ demodulator and the A/D converter, is plotted in Fig. 8. The rms value is 0.0067 degree for a 10-shot moving average data. This corresponds to 80 fs, which is sufficient for our requirement for SACLA.

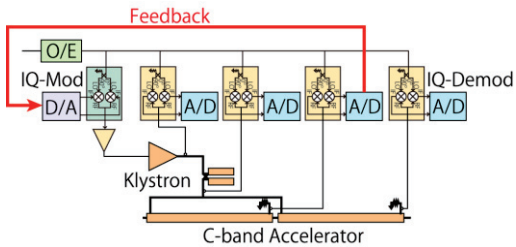

Figure 6: Schematic diagram of the LLRF system.

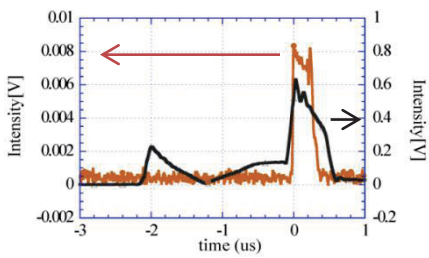

Figure 7: Rf amplitude waveforms detected by an IQ demodulator. The black curve shows an acceleration rf field of a C-band accelerator and brown one shows an beam-induced field when the klystron is off.

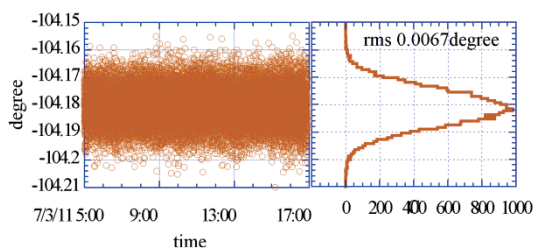

Figure 8: Trend graphs of the amplitude and phase of 238 MHz sub-harmonic buncher cavity. Each data point shows a 10-shot moving average.

Water-cooled Enclosures and Low-noise DC Power Supply

To keep the temperatures of all the electric circuits and PSOFs, we developed a water-cooled 19-inch rack and a water-cooled fiber duct [6]. Figure 9 shows a schematic drawing and a photograph of the water-cooled 19-inch rack, and Figure 10 shows those of the water-cooled fiber duct. The water-cooled rack is equipped with a heat exchanger, which regulates the temperature of circulating air by using cooling water within a ±0.2 K stability. The water-cooled duct consists of an inner steel duct having some water cooling channels and an outer steel duct. A thermal insulator is filled between the inner and outer ducts. PSOFs are installed in the inner ducts together with a thermal insulator.

The temperature stability of the water-cooled 19-inch rack is plotted in Fig. 11. The temperature inside the rack was kept within ±0.2 K as expected, while the ambient temperature showed a drift of 0.5 K. The temperature stability of the water-cooled fiber duct was also confirmed to be the same level as the water-cooled 19-inch rack.

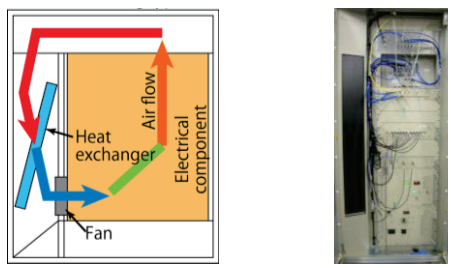

Figure 9: Cross-sectional top view of the water-cooled 19-inch rack (left) and a photograph of the rack (right).

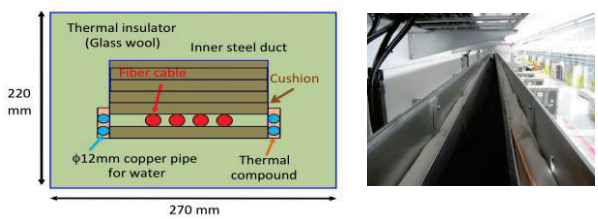

Figure 10: Schematic drawing of the water-cooled fiber duct (left) and a photograph of the duct (right).

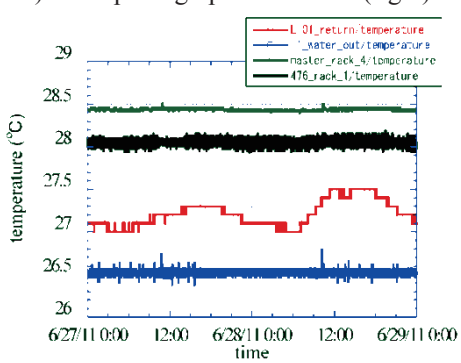

Figure 11: Temperature stability of a water-cooled 19-inch rack. Green and black lines indicate the temperature in the rack. Blue and red lines are the water temperature and the ambient temperature, respectively.

Copyright © 2013 CC-BY-3.0 and by the respective authors

ISBN 978-3-95450-145-8

We also developed a low-noise DC power supply for the rf electronics and VME data acquisition boards. The three-phase AC power is rectified and the voltage is stabilized by a precise linear regulator. The noise floor of the output voltage was measured to be -150 dBV/√Hz for 10–1000 Hz, except for the line frequency and its harmonics. Even for the line frequency, the amplitude was less than -100 dBV. The voltage stability was confirmed to be less than 10 ppm pk-pk).

BEAM DIAGNOSTIC INSTRUMENTS

We use following beam monitors in SACLA for precise beam diagnostics [7]: an rf cavity beam position monitor (RF-BPM), a beam profile monitor using OTR (Optical Transition Radiation) or YAG:Ce scintillation, a fast differential current transformer (CT), a C-band transverse rf deflecting cavity, a streak camera system, and a CSR (Coherent Synchrotron Radiation) monitor. In the following sub-sections, details of these monitors are described.

RF Cavity Beam Position Monitor

The RF-BPM cavity consists of two cylindrical cavity resonators, as shown in Fig. 12: a TM110 dipole resonator for the position detection and a TM010 monopole resonator for the phase reference and the bunch charge information. The resonant frequency is 4.76 GHz for both cavities. The signal from an RF-BPM is detected by an IQ demodulator.

We analyzed the position resolution of 20 RF-BPMs in the undulator section. The electron beam energy was 7 GeV and the bunch charge was 0.1 nC. The beam position at a given RF-BPM was estimated from the other 19 RF-BPMs and the position resolution was calculated from the rms of the difference between the measured value and the estimated one. Figure 13 shows a scatter plot of the measurement v.s. estimation. The measured position and estimated position were almost the same and the position resolution was calculated to be 0.5 μm [8].

Beam Profile Monitor

To obtain a transverse beam profile, we use a fluorescent screen and an optical transition radiation (OTR) screen [9]. The screen attached to a pneumatic actuator in order to insert into the beam orbit remotely. The radiation from the screen is focused by a custom-made lens system to a CCD camera, as shown in Fig. 14. The optical resolution of the lens system was confirmed to be 2 μm in case of the maximum magnification of x4.

The profile monitor works well for the bunch length longer than 100 fs. However, we encountered abnormal OTR radiation when the bunch length was less than 100 fs. This phenomenon is known as coherent OTR (C-OTR). Therefore, we changed the target from the OTR to the YAG:Ce in order to use scintillation light. Nevertheless, C-OTR was still observed from the YAG:Ce screen. We put an OTR mask in front of the lens, as illustrated in Fig. 15, since OTR is emitted in the forward direction. After that, an appropriate beam profile image was obtained, as shown in Fig. 16 [7].

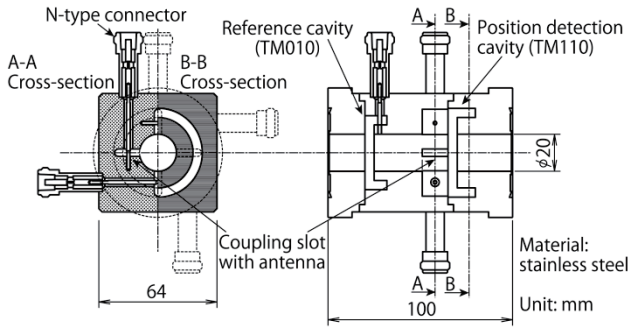

Figure 12: Drawing of the RF-BPM cavity.

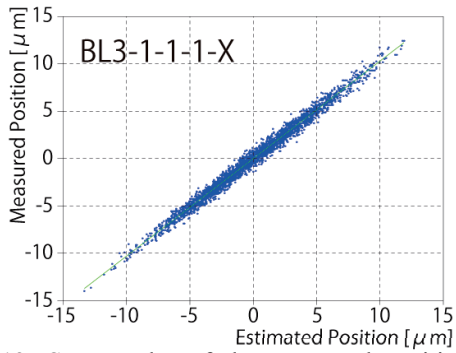

Figure 13: Scatter plot of the measured position of a BPM versus the estimated position from other BPMs.

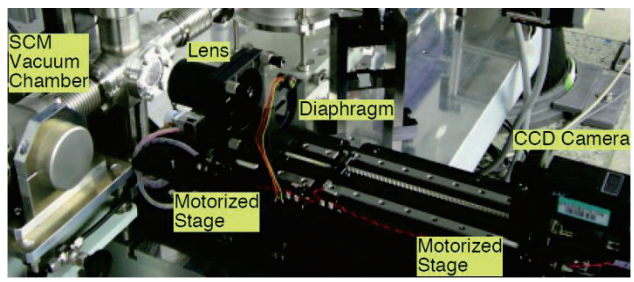

Figure 14: Photograph of the beam profile monitor.

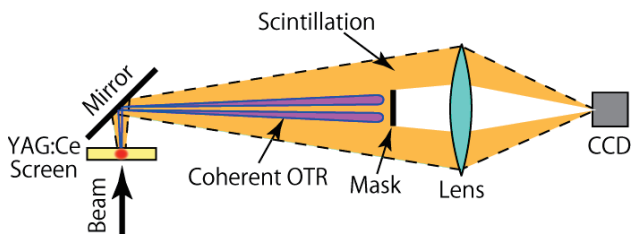

Figure 15: Setup of the profile monitor to mitigate C-OTR.

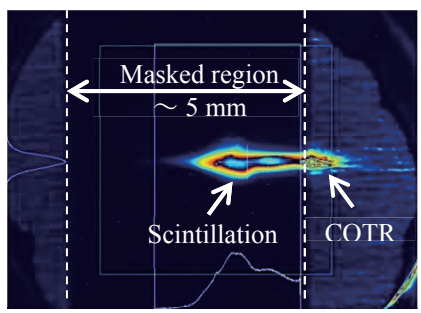

Figure 16: Beam profile image observed by the beam profile monitor with a YAG:Ce screen and an OTR mask.

ISBN 978-3-95450-145-8

Copyright © 2013 CC-BY-3.0 and by the respective authors

Fast Differential Current Transformer

We developed a high-speed differential CT [10], as shown in Fig. 17. This CT has four outputs: two are positive and the others are negative. By subtracting a negative signal from a positive one, we can remove any common-mode noise. Since a single-turn pickup coil is used, the rise time of the output pulse is expected to be small. Raw signal waveforms from the differential CT are plotted in Fig. 18. The rise time was 0.2 ns. Therefore, this CT has a capability to measure the bunch length longer than about 0.5 ns.

Transverse RF Deflector Cavity

We use a C-band transverse rf deflecting cavity (RFDEF) [11] to measure the temporal bunch structure of an electron beam. A schematic setup of the RFDEF system is shown in Fig. 19. An electron beam is swept by a transverse deflecting rf field and the temporal structure is converted to the transverse profile. The transverse profile is observed by a profile monitor with a spatial resolution of approximately 3μm.

Figure 20 shows a measured temporal bunch structure of a 1.4 GeV beam. The electron beam is vertically stretched by RFDEF. The temporal structure of a 100 fs long beam is appropriately obtained with approximately a 10 fs resolution.

Streak Camera

To measure a bunch length of longer than 300 fs, a streak camera system is also used. OTR light emitted by a stainless-steel foil is transmitted outside the accelerator tunnel and detected with a FESCA-200 [12] streak camera, which is located downstream of the BC3. Nevertheless, the bunch length after the BC1 or the BC2 can be also measured, since the BC2 and the BC3 can be bypassed.

Figure 21 shows an example of a measured bunch length after the BC2. The bunch length was 0.54 ps FWHM in this case. Thus, the streak camera system has a capability to measure the bunch length less than 1 ps.

Coherent Synchrotron Radiation Monitor

For a non-destructive bunch length monitor, a CSR monitor was developed [13]. A schematic view of the CSR monitor is illustrated in Fig. 22. CSR from the fourth dipole magnet of a bunch compressor chicane is reflected and extracted from the vacuum chamber. The CSR is then focused with a THz lens and detected with a pyro-electric detector.

Figure 23 shows a CSR intensity dependence on the bunch length. The bunch length was varied by the S-band accelerating rf phase upstream of BC2. In this data set, bunch lengths measured by the RFDEF system were 200 fs, 300 fs and 400 fs (FWHM) at -1, 0 and +1 degree, respectively. Here, the rf phase of 0 degree means the lasing condition of SACLA. Thus, the CSR monitor has sufficient sensitivity to the bunch length.

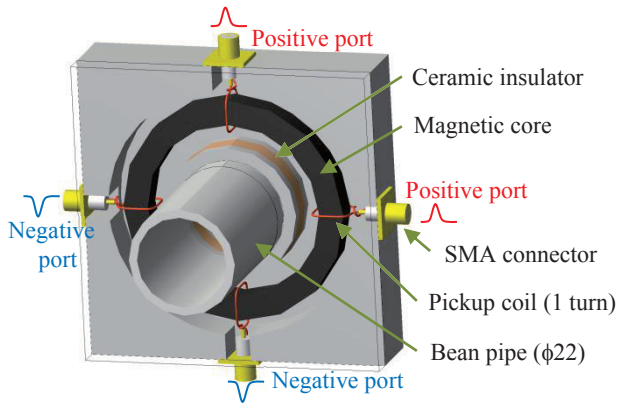

Figure 17: Schematic view of the differential CT.

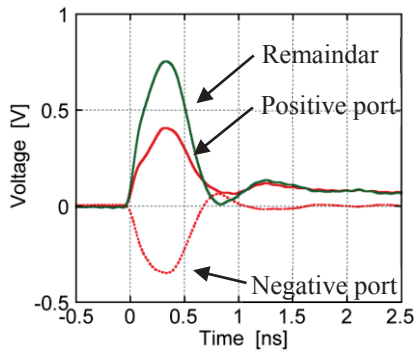

Figure 18: Waveforms of the differential CT.

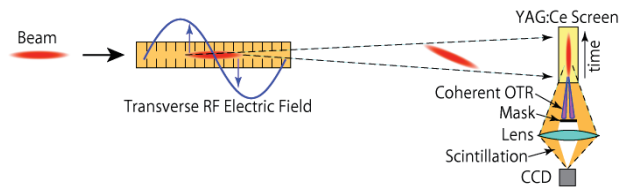

Figure 19: Schematic setup of the RFDEF system.

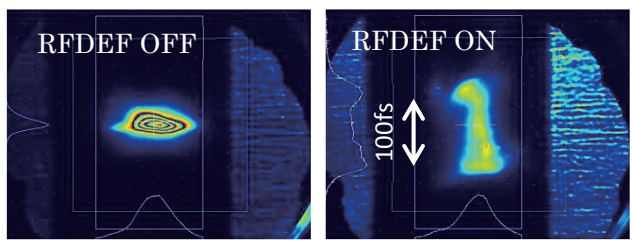

Figure 20: Beam profiles taken by the RFDEF system. The RFDEF is off in the left figure, and the RFDEF is on in the right one.

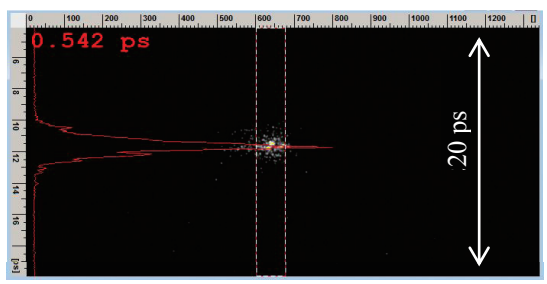

Figure 21: Example of a streak camera image. The temporal structure is stretched vertically. The full scale of the time range is 20 ps. The red line shows the projection of the image, which has the FWHM value of 0.54 ps.

Copyright © 2013 CC-BY-3.0 and by the respective authors

ISBN 978-3-95450-145-8

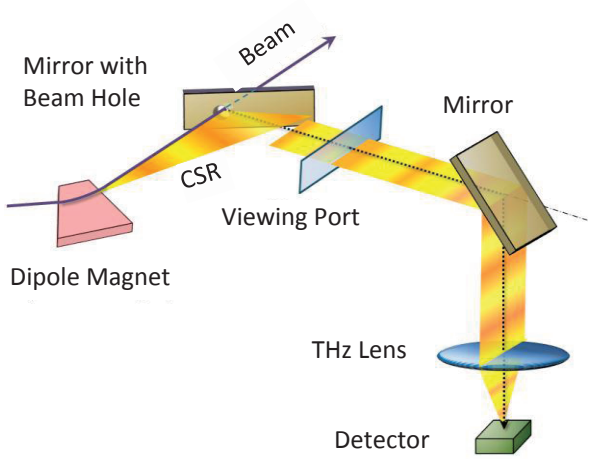

Figure 22: Schematic setup of the CSR monitor.

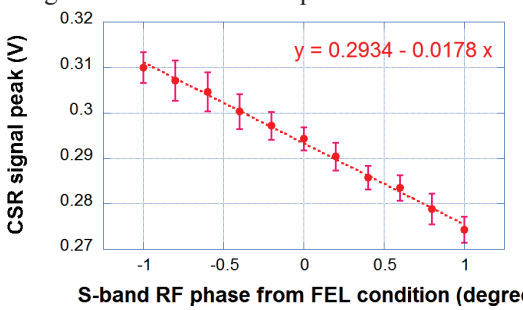

Figure 23: CSR intensity at BC2 as a function of the S-band acceleration rf phase. The origin of the horizontal axis is the phase at the XFEL lasing condition. Error bars represent the standard deviations of intensity fluctuations

POSSIBLE APPLICATIONS TO ERL

In this section, we briefly discuss some possible applications to an ERL about our synchronization and beam diagnostic system.

For the synchronization issue, the optical system can be applied to ERL. In the ERL case, the WDM part can be removed, since all accelerator cavities have the same frequency of 1.3 GHz. On the other hand, the LLRF system cannot be used in the ERL machine without any modifications, because our LLRF system is intended for pulsed rf signals, while an ERL uses CW signal. Moreover, our LLRF system does not have an intra-pulse feedback capability, while an ERL needs a fast feedback system.

For the beam diagnostic instrument, most of our non-destructive monitors can be applied, if the repetition rate is less than 10 MHz. Since the repetition rate of the SACLA is 60 Hz, our instruments are not applicable to a 1.3 GHz operation mode of an ERL. For example, the RF-BPM cavity can be a large impedance source, when the repetition rate is more than 10 MHz. If any low-repetition bunches can be extracted from the ERL ring, all of our monitors can be used including destructive monitors.

SUMMARY

We developed a synchronization system and a beam diagnostic system for the XFEL facility, SACLA. By using an optical rf and timing distribution system and IQ modulation/demodulation technique, acceleration rf phase and amplitude are precisely controlled. The time-equivalent value of a phase stability is less than 100 fs (rms). The optical system has capability to provide a timing signal to ERL. However, it is difficult to use our LLRF system to ERL without any modification.

For the beam diagnostics, we developed high-resolution monitors for both spatial and temporal measurements. The RF-BPM has sub-μm resolution, and the beam profile monitor can measure a beam size of around 10 μm. The temporal bunch structure can be measured for the bunch length from 30 fs to several picoseconds, by using a C-band rf deflector cavity, a streak camera and a CSR monitor. It is hard to use our beam monitors in an ERL ring with the repetition rate of 1.3 GHz. However, our monitors can be applied, if the repetition rate is reduced to 10 MHz or less.

REFERENCES

[1] H. Tanaka, *et al.*, "Status Report on the Commissioning of the Japanese XFEL at SPring-8", proceedings of IPAC'11 (2011).
[2] H. Maesaka, *et al.*, "Recent Progress of the RF and Timing System of XFEL/SPring-8", proceedings of ICALEPCS'09 (2009).
[3] N. Hosoda, *et al.*, "SCSS Prototype Accelerator Timing System", proceedings of APAC'07 (2007).
[4] M. Musha *et al.*, Appl. Phys. **B** 82, 555–559 (2006).
[5] T. Fukui *et al.*, "A Development of High-Speed A/D and D/A VME Boards for a Low Level RF System of SCSS", proceedings of ICALEPCS'05 (2005).
[6] N. Hosoda, *et al.*, "Construction of a Timing and Low-level RF System for XFEL/SPring-8", proceedings of IPAC'10 (2010).
[7] Y. Otake, *et al.*, "Commissioning and Performance of the Beam Monitor System for XFEL/SPring-8 'SACLA'", proceedings of IPAC'11 (2011).
[8] H. Maesaka, *et al.*, "Performance of the RF Cavity BPM at XFEL/SPring-8 'SACLA'", proceedings of FEL'11 (2011).
[9] K. Yanagida *et al.*, "Development of Screen Monitor with a Spatial Resolution of Ten Micro-meters for XFEL/SPring-8", Proc. of LINAC'08 (2008).
[10] S. Matsubara, et al., "Development of High-speed Differential Current Transformer Monitor", proceedings of IPAC'11 (2011).
[11] H. Ego, *et al.*, "Transverse C-band Deflecting Structure for Longitudinal Phase Space Diagnostics in the XFEL/SPring-8 'SACLA'", proceedings of IPAC'11 (2011).
[12] Hamamatsu Photonics K. K., http://www.hamamatsu.com/
[13] C. Kondo, *et al.*, "CSR Bunch Length Monitor for XFEL/SPring-8–SACLA", proceedings of IPAC'11 (2011).

ISBN 978-3-95450-145-8

Copyright © 2013 CC-BY-3.0 and by the respective authors